

Geophysical Research Letters

RESEARCH LETTER

10.1029/2021GL092547

Key Points:

- Observed broadening of the droplet size distribution (DSD) is consistent with droplet growth processes that accelerate precipitation formation
- Sedimentation rates inferred from DSDs show strong correlation with maximum precipitation rates and rain water paths
- Multi-angular polarimetry can be used to remotely study cloud top bimodal size distributions and precipitation onset

Supporting Information:

Supporting Information may be found in the online version of this article.

Correspondence to:

K. Sinclair,
kenneth.sinclair@nasa.gov

Citation:

Sinclair, K., van Diedenhoven, B., Cairns, B., Alexandrov, M., Dzambo, A. M., & L'Ecuyer, T. (2021). Inference of precipitation in warm stratiform clouds using remotely sensed observations of the cloud top droplet size distribution. *Geophysical Research Letters*, 48, e2021GL092547. <https://doi.org/10.1029/2021GL092547>

Received 19 JAN 2021
 Accepted 3 MAY 2021

Inference of Precipitation in Warm Stratiform Clouds Using Remotely Sensed Observations of the Cloud Top Droplet Size Distribution

Kenneth Sinclair^{1,2} , Bastiaan van Diedenhoven³ , Brian Cairns¹, Mikhail Alexandrov³, Andrew M. Dzambo⁴ , and Tristan L'Ecuyer⁵

¹NASA Goddard Institute for Space Studies, New York, USA, ²Universities Space Research Association (USRA), Columbia, MD, USA, ³Columbia University, New York, USA, ⁴University of Oklahoma, Cooperative Institute for Meteorological Mesoscale Studies, Norman, OK, USA, ⁵University of Wisconsin, Madison, WI, USA

Abstract Drizzle is a common feature of warm stratiform clouds and it influences their radiative effects by modulating their physical properties and lifecycle. An important component of drizzle formation are processes that lead to a broadening of the droplet size distribution (DSD). Here, we examine observations of cloud and drizzle properties retrieved using colocated airborne measurements from the Research Scanning Polarimeter and the Third Generation Airborne Precipitation Radar. We observe a bimodal DSD as the aircraft transects drizzling open-cells whereby the larger mode reaches a maximum size near cloud center and the smaller mode remains relatively constant in size. We review similarities between our observations with droplet growth processes and their connections with precipitation onset. We estimate droplet sedimentation using the cloud top DSD and find a correlation with rain water path of 0.82. We also examine how changes in liquid water paths and droplet concentrations may act to enhance or suppress precipitation.

Plain Language Summary Low clouds play a central role in regulating Earth's climate by reflecting a portion of incoming sunlight back to space. When clouds rain, the amount of sunlight reflected back to space is altered because the distribution and amount of water within a cloud is modified. Detecting the presence of rain using passive instruments is challenging. In this study, we use a multi-angular polarimeter and radar instruments to investigate how droplets at cloud top relate to rainfall that occurs lower in the cloud. We observe a pattern in droplet sizes that appears to be related to rainfall formation, and we discuss commonalities this pattern has with rainfall formation processes. We investigate several key cloud properties and how they can be used to determine rainfall rates. This work may help future passive space-based instruments determine if a cloud is raining and improve the accuracy of cloud property retrievals.

1. Introduction

Low stratiform clouds cover approximately one third of Earth's surface and substantially enhance the shortwave radiative effect (Klein & Hartmann, 1993). The shortwave radiative effects of these clouds are determined by macrophysical properties such as cloud coverage and liquid water paths (LWPs) as well as microphysical properties that relate to their droplet size distributions (DSDs). Precipitation influences these clouds' macro- and micro-physical properties and thereby their radiative effects. Precipitation amount and rates are in turn governed by a large number of microphysical, thermodynamic and dynamical processes (Austin et al., 1995; Wood, 2005a). For example, studies have found that drizzle rates correlate positively with cloud water content and droplet sizes (Lebsock et al., 2011; Takahashi et al., 2017) and negatively with droplet concentrations (Nd; Austin et al., 1995; Comstock et al., 2004; Khairoutdinov & Kogan, 2000). It follows that enhanced aerosol concentrations may suppress drizzle by increasing droplet concentrations, thereby altering the rate that precipitation forms. These effects may modulate the amount and distribution of remaining liquid water leading to changes in the cloud lifecycle (Albrecht, 1989). However, many of these processes are complex and coupled, making it challenging to study individual effects.

An important component of precipitation formation are droplet growth processes that lead to spectral broadening of the DSD (Brenguier & Choumat, 2000). It is well-established that gravitational collision and

coalescence processes initiate precipitation in liquid water clouds and these processes act most effectively for droplets with radii larger than $40\ \mu\text{m}$ (Pruppacher & Klett, 2010). Prior to reaching this size, diffusional growth processes readily produce droplets up to $\sim 10\ \mu\text{m}$, and up to $20\ \mu\text{m}$ over longer ($\sim 103\ \text{s}$) timeframes (Wallace & Hobbs, 2006). Diffusional growth rates decrease rapidly with increasing droplet size because the rate that droplet sizes increase are inversely proportional to cube of the radius. Droplet growth through diffusion and gravitational collision and coalescence processes is inefficient between ~ 10 and $25\ \mu\text{m}$, a range termed the “growth gap”, which results in precipitation being unable to form on timescales as short as those observed ($\sim 103\ \text{s}$) (Curry & Webster, 1998; Falkovich et al., 2002; Grabowski & Wang, 2013). Hence, additional processes are required to develop precipitation on timescales that are observed. However, the physical mechanisms that lead to rapid precipitation onset are a significant source of uncertainty in cloud physics (Hsieh et al., 2009; Morrison et al., 2020).

Many studies have investigated the role various processes have in enhancing the rate of formation of large droplets, which include secondary nucleation (Segal, et al., 2003), inhomogeneous entrainment-mixing (Baker et al., 1980; Brenguier & Grabowski, 1993) and turbulent collision-coalescence (Falkovich et al., 2002), amongst many others. These processes can significantly enhance collision efficiency by a factor of 2–4, increasing droplet growth rates through the “growth gap” and enabling precipitation to form on timescales that align with observations (Berry & Reinhardt, 1974; Falkovich et al., 2002; M. B. Pinsky et al., 2007).

A common effect of these processes is spectral broadening of the DSD and in some cases the development of bimodal droplet distributions (Grabowski & Wang, 2013; Segal, et al., 2003). A number of studies have found evidence of bimodal DSDs (Korolev, 1994, 1995; Lasher-trapp et al., 2005; Prabha et al., 2011; Warner, 1969a, 1969b). Observational studies investigating spectral broadening processes and drizzle formation primarily rely on *in situ* cloud probes (Hudson & Yum, 1997). However, *in situ* measurements are spatially and temporally averaged, which can either enhance or diminish a secondary mode (Segal et al., 2003).

Additional observational studies linking microphysical processes and precipitation are identified as a key requirement needed to improve and incorporate additional model parameterizations of precipitation processes (Morrison et al., 2020). Remotely sensed observations of the DSD along with other innovative measurement techniques may enable further progress in this area (e.g., Grabowski & Wang, 2013).

In this study, we investigate connections between remotely sensed cloud top DSDs and precipitation in open-cell stratiform clouds. We examine a bimodal feature in the DSD that exhibits a recurring pattern as the aircraft transects precipitating cells. Sedimentation rates are estimated using cloud top DSDs and connections to precipitation rates retrieved from cloud radar observations are discussed. We examine how changes in droplet number concentration (Nd) and LWP may act to enhance or suppress precipitation rates.

2. Data and Methods

Observations of precipitating stratiform clouds were made during the third deployment of NASA's Observations of Aerosols Above Clouds and their Interactions (ORACLES) campaign (Redemann et al., 2020). This deployment took place in the South East Atlantic region, which features one of the largest persistent subtropical marine cloud decks in the world and is subject to annual variations in aerosol loading from Southern Africa biomass burning emissions. This study uses flight data from 10/2/2018, which focused on low stratiform cloud microphysics so the aircraft sampled clouds with remote sensing legs and sampled them *in situ* at a range of altitudes. These observations include precipitating open and closed cells. Satellite imagery of clouds sampled along with the flight path are shown in Figure S1 and aircraft camera imagery is shown in Figure S2.

Cloud retrievals are made using the airborne Research Scanning Polarimeter (RSP; Cairns et al., 1999), which makes polarimetric and total intensity measurements across nine spectral bands. The RSP makes 152 measurements every 0.82 s at viewing angles spaced 0.8° apart, effectively sweeping about $\pm 60^\circ$ from nadir along the aircraft's track. Its instantaneous field of view is 14 mrad (0.8°). Aboard an aircraft, consecutive scans view the same location from multiple viewing angles, which are aggregated into virtual scans at cloud top (Alexandrov, Cairns, Emde, et al., 2012; Sinclair et al., 2017). This allows the RSP to observe the

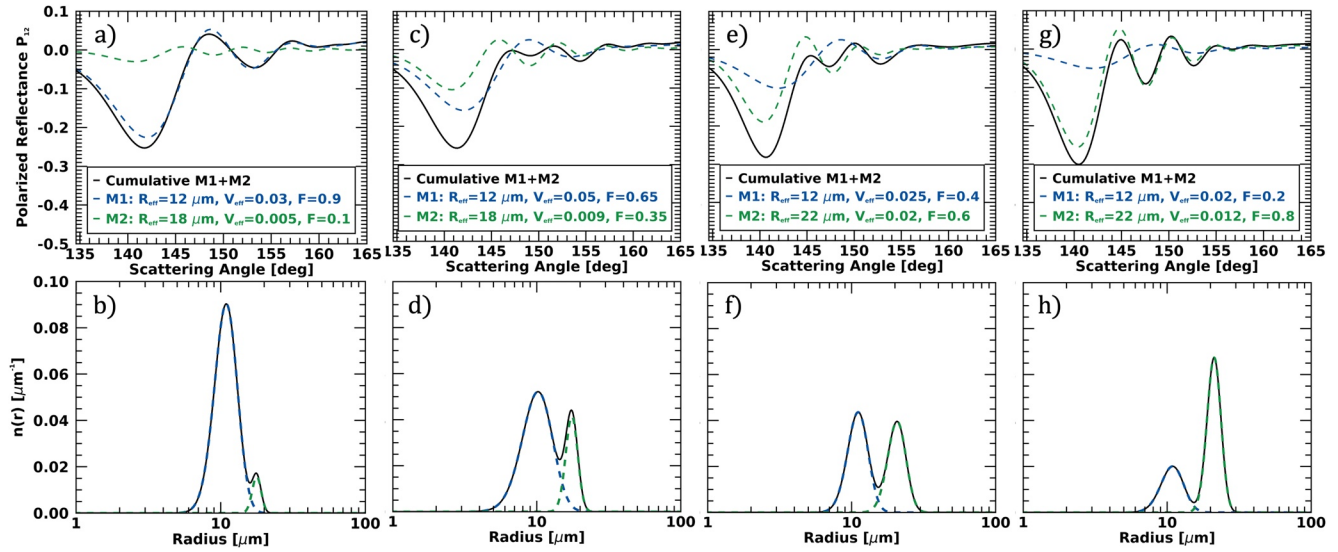


Figure 1. Top: Polarized reflectance observed in the scattering plane for a bimodal droplet distribution (black) with individual components (green and blue dashed). Bottom: Inverse Fourier transform of polarized reflectance showing total droplet size distribution (DSD) (black) and individual modes (blue and green) used to compute polarized reflectances.

sharply defined cloudbow feature originating from single-scattered light between scattering angles of 135° and 165° . The Rainbow Fourier Transform (RFT; Alexandrov, Cairns, & Mishchenko, 2012) method uses these observations of the cloudbow to retrieve the DSD without a priori assumptions about its functional shape. The shape of the cloudbow is determined by single scattering properties of droplet, allowing it to be modeled using Mie theory. Simulations have shown RFT is capable of retrieving bimodal or even theoretical rectangular distributions (Alexandrov et al., 2020; Alexandrov, Cairns, & Mishchenko, 2012). To identify and characterize bimodal distributions, we assume each mode is of gamma distribution shape (viz., Hansen & Travis, 1974), fit one or more modes to the area distribution and calculate the effective radius (r_{eff}) and effective variance (v_{eff}) of each. To minimize overfitting, our implementation of the RFT retrieval does not fit secondary modes that account for less than 0.1 of the fractional DSD area.

Since it is the relative shape and not intensity of the cloudbow feature that contains information on the DSD, these retrievals are robust in cases affected by three-dimensional radiative transfer effects, multilayered or broken cloud structures and above-cloud aerosol layers (Alexandrov, Cairns, Emde, et al., 2012; Miller et al., 2018), in contrast to techniques based on shortwave reflectance measurements (e.g., Nakajima & King, 1990). Comparisons with Large Eddy Simulations show the RFT method is capable determining r_{eff} , v_{eff} and the relative weights of each mode for bimodal distributions (Alexandrov et al., 2020). These LES results show the total r_{eff} values generally agree within $0.5 \mu\text{m}$ and v_{eff} within 0.05 (Alexandrov et al., 2020). The retrieved DSD generally pertains to a depth of about 1 optical depth from cloud top (Alexandrov et al., 2018; Miller et al., 2018).

Examples of simulated polarized reflectance and corresponding DSDs are shown in Figure 1. Total polarized reflectance is a convolution of polarized reflectances from individual modes within the distribution (Figures 1a, 1c, 1e, and 1g). Applying the inverse Fourier transform allows individual modes to be deconvolved from the signal (Figures 1b, 1d, 1f, and 1h).

Retrieval of the full DSD at cloud top allow estimations of the total droplet sedimentation rate, R , to be estimated using:

$$R = \frac{4\pi\rho_w N_d}{3} \int_0^\infty w_T r^3 n(r) dr \quad (1)$$

where n is the normalized DSD retrieved using RFT, r is the droplet radius, ρ_w is the density of liquid water ($\rho_w = 1000 \text{ kg / m}^3$), $w_T(r)$ is the terminal velocity in m s^{-1} calculated from a fourth-order polynomial fit

with respect to r using the full Reynolds number approach described in Pruppacher and Klett (1997). N_d is the droplet concentration and is estimated using Equation 2 below. This sedimentation rate is analogous to precipitation rates (Wood, 2005b). Equation 1 has units of $kg\ m^{-2}\ s^{-1}$, which we then convert to $mm\ m^{-2}\ hr^{-1}$ by assuming 1 kg water equals 1 dm^3 and multiplying by $3600\ s\ hr^{-1}\ mm\ m^{-2}\ kg^{-1}$.

Precipitation rates also correlate to the ratio of LWP and N_d (Austin et al., 1995; Comstock et al., 2004). Here we use the retrieved effective radius and cloud optical thickness, τ_c , to infer N_d using:

$$N_d = \frac{\sqrt{5}}{2\pi k} \left(\frac{f_{ad} c_w \tau_c}{Q_{ext} \rho_w r_e^5} \right)^{1/2} \quad (2)$$

where f_{ad} is the fraction adiabaticity ($f_{ad} = 0.6$), c_w is the condensation rate ($c_w = 3.0\ g\ /\ m^4$), Q_{ext} is the extinction efficiency factor ($Q_{ext} = 2.0$), k is the ratio of volume mean radius to effective radius ($k = 0.8$), τ_c is the retrieved cloud optical thickness and r_e is the retrieved effective radius (Grosvenor et al., 2018). RSP retrieves optical depth by measuring radiometric reflection at nadir in the nonabsorbing 864 nm band and using a look up table created with a plane-parallel radiative transfer model (cf. Nakajima & King, 1990). Here we rely on using constant values of f_{ad} and c_w due to spatiotemporal differences between in situ and remote sensing measurements. This N_d retrieval requires assumptions of the cloud structure, which include a linearly increasing LWC profile and a constant droplet distribution relative width. Furthermore, LWP is inferred using (Grosvenor et al., 2018):

$$LWP = \frac{5}{9} \rho_w r_e \tau_c \quad (3)$$

For both N_d and LWP retrievals, we use RSP's r_e calculated using polarized reflectances from the RFT retrieval. Note that the LWP/N_d is then proportional to $\tau_c^{0.5}$ and $r_e^{3.5}$.

Precipitation retrievals are made using the Third Generation Airborne Precipitation Radar (APR-3; Dzambo et al., 2019), which flew aboard NASA's P-3 aircraft during ORACLES-3. APR-3 is a triple-wavelength radar system with Ku- (13 GHz) and Ka- (35 GHz) and W- (95 GHz) band frequencies that measure radar reflectivity, Doppler velocity and spectrum width. The W-band channel can detect drizzle sized droplets down to a reflectivity of -30 dBZ. APR-3 has a 0.9° field of view, which minimizes multiple scattering effects. The DSD's functional shape is derived from observational studies and parameterized as an exponential function for single moment microphysics schemes (Abel & Boutle, 2012), which introduces some uncertainty to the LWC and precipitation rate retrievals (e.g., Dzambo et al., 2020; Lebsock & L'Ecuyer, 2011). For this study we exclusively use the W-band to retrieve precipitation rate (R), maximum precipitation rate within the column (R_{max}), liquid water content and rain water content through the column using an optimal estimation technique adapted from the CloudSat 2C-RAIN-PROFILE (2C-RP) algorithm (Dzambo et al., 2020; L'Ecuyer & Stephens, 2002). We compare RSP observations with R_{max} and rainwater paths (RWPs) for convection and because cloud top retrievals of R are highly variable. Throughout this campaign, APR-3 retrievals are affected by near-surface noise in the lowest six bins (~ 210 m), which are not included in precipitation retrievals (Dzambo et al., 2019).

3. Results

On 10/2/2018 the P-3 aircraft transected several precipitating warm stratiform clouds between 12.0 and 12.15 decimal hour UTC (i.e., 12:00 and 12:09 UTC, see Figure 2). We show three selected cases where cloud top DSDs exhibit a recurring transition between monomodal and bimodal sharing attributes that include they are precipitating open-cell clouds with well-defined edges and have columnar rainwater paths (RWPs; Figure 2a) that increase from low values near cloud edge ($\sim 1\ g\ m^{-2}$) to relatively high values near cloud center ($\sim 35\ g\ m^{-2}$).

The first example occurs from ~ 12.12 to 12.13 UTC (Figure 2) and the DSD is initially monomodal near cloud edge (Figure 3a). This initial single smaller mode (M1) has a reff of $\sim 13.2\ \mu m$ with a corresponding

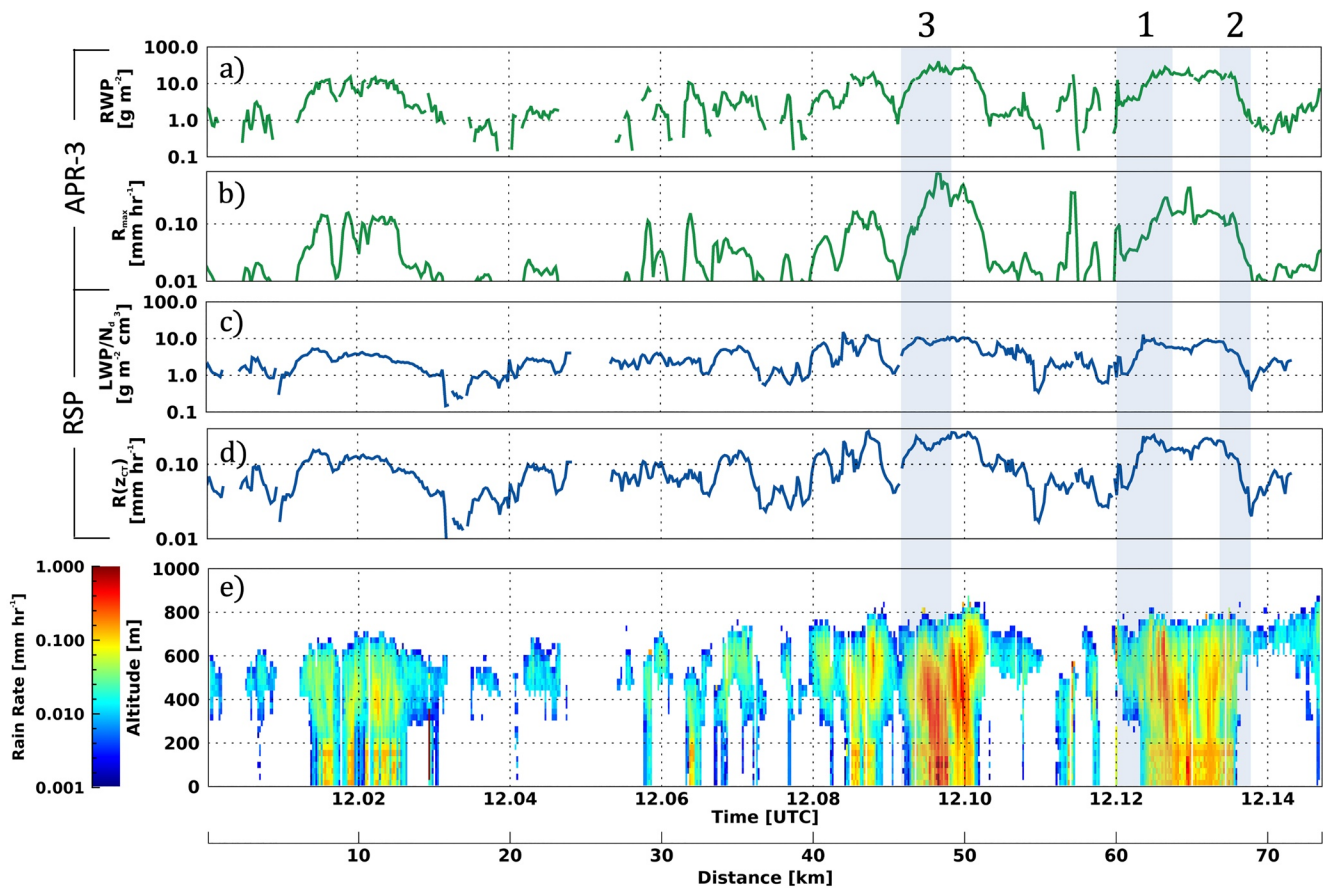


Figure 2. Precipitation retrievals on 10/2/2018 between 12.0 and 12.15 UTC. (a) APR-3 RWP (b) APR-3 column maximum precipitation rate (c) Research Scanning Polarimeter (RSP) derived liquid water path (LWP)/ N_d metric (d) RSP sedimentation rates (e) APR-3 precipitation rates.

columnar RWP of 2 g m^{-2} . A larger secondary mode (M2) emerges in the proceeding retrieval (Figure 3b) and a transition in the DSD occurs over $\sim 3.5 \text{ km}$ (26 observations) as the aircraft advances toward cloud center. Eleven DSDs from this transition are selected and shown in Figure 3. Throughout the transition, M1 maintains a relatively constant size while M2 increases in size from 17.6 to $\sim 21 \mu\text{m}$ and increases in fractional amount of the DSD.

This transition coincides with an $\sim 18 \text{ g m}^{-2}$ increase in columnar RWP. Toward cloud center, M2 becomes the dominant mode exceeding 0.9 of the fractional area and the DSD again becomes monomodal. This coincides with the most heavily precipitating portion of the cloud. In each example, the most heavily precipitating portion of these open-cell clouds contain a monomodal DSD with large r_{eff} . Furthermore, during this flight transect retrieved N_d decreases precipitously from $\sim 60 \text{ cm}^{-3}$ near the cloud edge to 20 cm^{-3} near cloud center and LWP increases from about 50 g m^{-2} near cloud edge to over 200 g m^{-2} near center. Time series of N_d , LWP and other cloud properties from 12.0 to 12.15 UTC are shown in Figure S3. Precipitation formation processes, including accretion and autoconversion, are both associated with decreases in N_d , which we discuss later (M. Pinsky et al. 2001).

The presence of these bimodal DSDs is supported by *in situ* measurements by the Phase Doppler Interferometer (PDI). Figure 3l shows the average of 59 measurements made within 100 m of cloud top from four profiles during a sawtooth leg between 13.05 and 13.25 UTC on 10/2/2018. These measurements exhibit a similar bimodal structure in the DSD with modes M1 and M2 having r_{eff} of ~ 8.6 and $16.0 \mu\text{m}$, respectively. As a result of using a single aircraft, these *in situ* measurements were made 27 km away and $\sim 1 \text{ h}$ after the remote sensing measurements. Averaging measurements can enhance or diminish a secondary mode (Segal

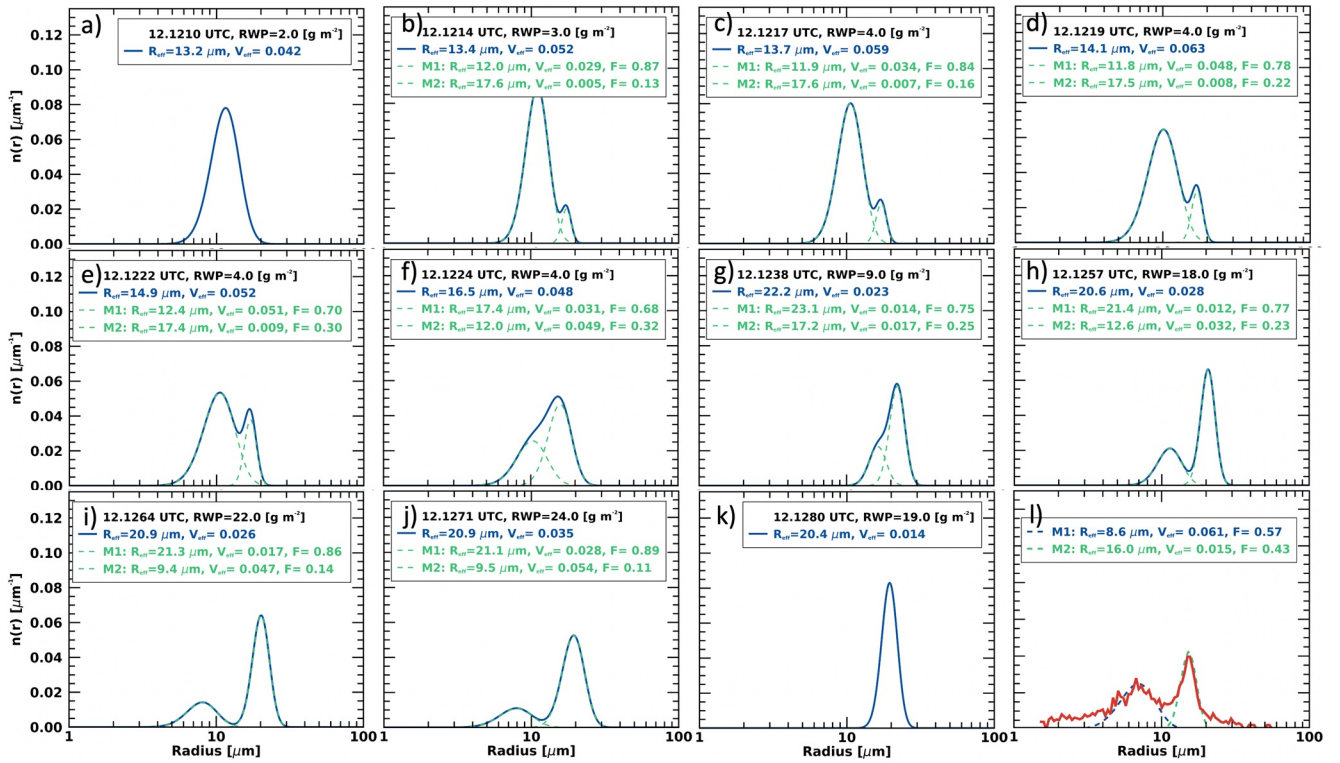


Figure 3. (a–k) Observed cloud top total droplet size distributions (DSDs) (blue) and individual modes M1 and M2 (dashed green) from 11 retrievals selected from a 4 km track where the aircraft approaches the center of a precipitating low stratiform cloud. The rainwater paths (RWP) inferred by APR-3 is given in the legend, along with effective radius and effective variance of the total DSD and the two modes (l) *In situ* measurements made near cloud top by the Phase Doppler Interferometer (PDI) instrument.

et al., 2003). Furthermore, a previous study found an approximate 5 μm discrepancy between PDI and a Forward Scattering Spectrometer Probe retrievals of cloud DSDs (Chuang et al., 2008).

A second example occurs as the aircraft exits a precipitating core and the transition occurs in reverse from ~ 12.13 to 12.14 UTC (Figure 2; Figure S4). The DSD is initially monomodal with a dominant M2 mode, and M1 reappears and keeps a nearly constant size of $12 \mu\text{m}$ but increases in fractional DSD area until the aircraft passes the cloud edge. Through this transition, M2 decrease from 23 to $20 \mu\text{m}$. Spanning 2 km , this transition is the shortest of the three cases. In this case, APR RWP decreases from ~ 18 to 2 g m^{-2} . During this transition, N_d increases from about 18 cm^{-3} near cloud center to 55 cm^{-3} near cloud edge.

A third example occurs earlier in the transect from ~ 12.09 to 12.10 UTC (Figure 2; Figure S5). This transition is very similar to the first example with the smaller M1 being initially dominant to the larger M2 mode, but the transition occurs over a shorter span of $\sim 3 \text{ km}$. Unlike the example 1, M1 does increase slightly from 11.6 to $13.7 \mu\text{m}$, and leaps to $16.4 \mu\text{m}$ in the last retrieval. M2 consistently grows from $18.6 \mu\text{m}$ initially to $\sim 25 \mu\text{m}$. This transition corresponds to RWP increases from 2 to 25 g m^{-2} . A more moderate decrease of N_d is observed from about 40 cm^{-3} near the cloud edge to 20 cm^{-3} near cloud center and LWP again increases from about 30 to 150 g m^{-2} near cloud center.

We use RSP's cloud top DSD to infer precipitation rates according to Equation 1 (Figure 2d). All colocated retrievals from the entire 12.00 – 12.15 UTC flight leg are used and a boxcar smoothing function is used on precipitation rate estimates over three retrievals. Interestingly, RSP-derived precipitation rates show good covariability with maximum column precipitation rates measured by APR-3 (Figure 4a). We find a correlation between $R(z_{CT})$ and R_{max} of 0.68 and the relationship can be approximated using the parameterization:

$$R_{max} \approx 1.36 \cdot R(z_{CT})^{1.48} \quad (4)$$

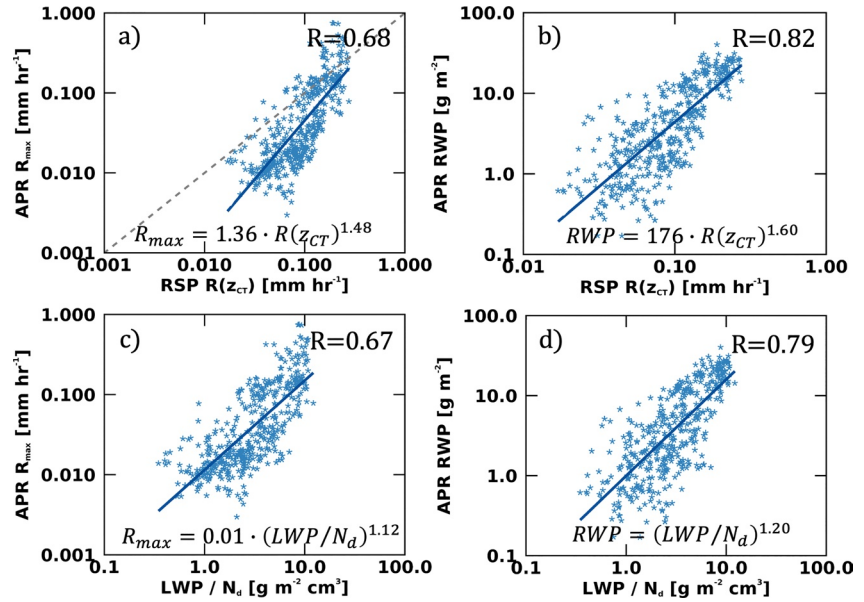


Figure 4. Scatterplots with correlations shown in top right and least squares fit on the bottom of: (a) RSP $R(z_{CT})$ versus APR-3 R_{max} (b) $R(z_{CT})$ RSP $R(z_{CT})$ versus APR-3 RWP (c) RSP LWP/N_d versus APR-3 R_{max} (d) RSP LWP/N_d versus APR-3 RWP.

where $R(z_{CT})$ and R_{max} are both measured in mm hr^{-1} . Interestingly, $R(z_{CT})$ overpredicts precipitation in lightly drizzling cases. We do not expect RSP cloud top precipitation rates to entirely agree with APR-3's R_{max} since a number of factors are unaccounted for that would influence precipitation rates, such as updraft velocities. However, the correlation suggests the cloud top DSD contains some information on precipitation.

Interestingly, we find that precipitation rates estimated using the cloud top DSD have a stronger connection with total column RWP in units of g m^{-2} (Figure 4b) with a correlation of 0.82 and a relationship that can be approximated using the parameterization:

$$RWP \approx 176 \cdot R(z_{CT})^{1.60} \quad (5)$$

We also investigate connections between the LWP / N_d metric and APR-3 maximum column precipitation rate, R_{max} and RWP (Figures 4b and 4c). We find a correlation of 0.67 between R_{max} and LWP / N_d , which can be best described using the parameterization:

$$R_{max} \approx 0.012(LWP / N_d)^{1.12} \quad (6)$$

where R_{max} is in mm hr^{-1} , N_d is in cm^{-3} and LWP is in g m^{-2} . Furthermore, we find a correlation of 0.79 between RWP and LWP / N_d and the relationship is best approximated by the expression:

$$RWP \approx 1.00(LWP / N_d)^{1.20} \quad (7)$$

where RWP is in g m^{-2} . Consistent with prior studies such as Albrecht (1989) and references therein, these findings support the theory that precipitation has some dependence on droplet concentration, and higher N_d values may weaken the overall precipitation rate for a given LWP.

These transitions and correlations observed in open-cell stratiform clouds can be contrasted with closed-cell drizzling and nondrizzling flight legs where a well-defined single mode is routinely observed. In one such closed-cell example from 10.52 to 10.68 UTC on 10/7/2018, cloud top reff is small and remarkably constant varying only between 10.6 and 11 μm with a corresponding RWP that varies between 6 and 13 g m^{-2} . DSDs

selected from a portion of this transect on 10/7/2018 are shown in Figure S6 and the APR-3 precipitation rates are shown in Figure S7. We find comparatively low correlation between $R(z_{CT})$ and R_{max} of 0.24 and a correlation of 0.33 between $R(z_{CT})$ and RWP. APR-3 precipitation rates indicate drizzle occurs in lower portions of the cloud deck, which removes any indication of precipitation formation from the cloud top DSDs.

4. Discussion and Conclusions

In each of the three cases presented, a consistent pattern in the cloud top DSD is observed in shallow precipitating open-cell clouds over a range of 2–5 km. Near cloud edge, the DSD initially consists of a single cloud droplet-sized mode. A larger mode emerges toward cloud center and its fractional area of the DSD increases until the DSD again becomes monomodal consisting of just the large mode near the most heavily precipitating portion of the cloud. In each case, the DSD transition coincides with significant cloud property changes including decreases in droplet concentration and increases in LWP and RWP. Columnar RWPs increase by an order of magnitude through each transition.

This larger mode is interstitially sized between cloud and precipitation sized droplets. Estimates of threshold radii separating cloud and precipitation vary and range from 20 μm (Wood, 2005b), to 25 μm (Khairoutdinov & Kogan, 2000), to 40 μm (Beheng, 1994) and 50 μm (Long & Manton, 1974) amongst others. Recently, a third, medium-sized mode existing between 20 and 40 μm was introduced and found to improve autoconversion parameterization (Kogan & Ovchinnikov, 2020). Here we characterize the larger mode as medium-sized or drizzle-sized and recognize its correspondence with precipitation leaves open the possibility that the droplets are cloud top precipitation embryos. However, we cannot definitively characterize this larger mode as either a secondary cloud mode or precipitation mode.

We found high correlation between RSP derived cloud top sedimentation and RWP ($R = 0.82$) as well as precipitation rates ($R = 0.68$). These high correlations suggest there is additional information in the shape of the DSD that can be used to determine the amount of rain water in the column. This finding supports a recent observational study that found precipitation rates positively correlate with the width of the DSD, which used the RSP and a ship-based Precipitation Sensor (Sinclair et al., 2020). The 1:1 offset in Figure 4a can be partially due to low values of the cloud top sedimentation including mass from the smaller M1 or cloud mode in the RSP sedimentation calculation. Our findings of precipitation having a connection to LWP and N_d are in general agreement with prior empirical studies (Comstock et al., 2004; Pawlowska & Brenguier, 2003). We found that high values of LWP and low N_d values are associated with stronger precipitation, which supports the theory that increases in aerosol concentrations suppress drizzle formation (Albrecht, 1989; Liou & Ou, 1989).

Bimodal DSDs have been repeatedly observed in warm marine stratiform clouds (Korolev, 1994, 1995; Lasher-trapp et al., 2005; Prabha et al., 2011; Warner, 1969a, 1969b) and their presence has been linked to processes that enhance precipitation formation (Pinsky & Khain, 2002). Consistent with our observations, these processes result in the cloud mode being depleted through accretion into the drizzle mode (Khain & Pinsky, 2018). Once a larger droplet mode is formed, these collection processes become continuous, which reduces cloud-water and N_d as observed here (Berry & Reinhardt, 1974; Grabowski & Wang, 2013; Wood, 2005b). These results are in contrast with closed-cell lightly drizzling clouds where well-defined, small, single modes are routinely observed at cloud top. For the closed-cell cases, drizzle occurs lower in the cloud and there is no indication of precipitation formation at cloud top. Future integrative studies that combine polarimetric, radar and *in situ* observations are necessary to explore these findings more and will lead to a better understanding of precipitation processes.

Berry and Reinhardt (1974) evaluate precipitation formation through solutions to the stochastic collection equation that result in bimodal distributions through three processes, namely M1-M1 autoconversion, M1-M2 accretion and M2-M2 large hydrometer self-collection. Interestingly, their findings share several commonalities with our observations that include: (1) the smaller mode decreasing in droplet number but remaining approximately constant in size; (2) the larger mode increasing in concentration and size; (3) this process continuing until the smaller mode is depleted. A notable difference is the absence of droplets with radii greater than 25 μm in our observations. We postulate that we do not observe these large droplets because they sediment out of the highest region of the cloud where RSP observes the polarized signal. While

the RSP does retrieve r_{eff} larger than 30 μm , no study has yet validated the RFT retrieval on droplets in this size range (cf. Alexandrov et al., 2018, 2020), leaving the possibility that the RSP may be partially insensitive to droplets in this range.

Identifying the presence of precipitation is useful for remote sensing of cloud optical properties. For example, the presence of multiple modes in the DSD biases bi-spectral droplet size retrievals (Nakajima et al., 2010a). Furthermore, precipitation also causes subadiabaticity, which impacts space-based N_d retrievals (Grosvenor et al., 2018). To identify scenes that may be precipitating, some studies implement an r_{eff} threshold (Painemal & Zuidema, 2011; Nakajima et al., 2010b). Our findings indicate that precipitation in shallow stratiform clouds can be better distinguished using either the LWP / N_d relation or estimated $R(z_{CT})$ precipitation rates. If these properties are unavailable, cloud optical thickness is found to correlate better with RWP and R_{max} than polarimetric r_{eff} and bi-spectral r_{eff} retrievals. The bi-spectral r_{eff} consistently has the lowest correlation with all precipitation retrievals, even after removing low COT values. Table S1 shows the correlation between precipitation and several cloud optical properties including r_{eff} and optical thickness.

In the near future, it will be possible to conduct similar precipitation-related studies as those presented here using the space-based Hyper-Angular Rainbow Polarimeter-2 (HARP-2; Martins et al., 2018; McBride et al., 2019) of the NASA the Plankton, Aerosol, Cloud, ocean Ecosystem mission (Werdell et al., 2019). HARP-2 has sufficient angular resolution to apply the RFT on single pixels of ~ 5 km resolution, which will allow the shape of the DSD as well as N_d and LWP to be retrieved. This will allow RWP and precipitation rates to be inferred using the methods presented here. Note, however, that the HARP-2 spatial resolution is of similar order as the transitions in bimodal DSDs that we present here, so its ability to observe similar transitions will need to be assessed.

Data Availability Statement

Data used in this studies was acquired during NASA ORACLES and is available in the public repository at: <https://espo.nasa.gov/oracles/archive/browse/oracles>.

Acknowledgments

The authors gratefully acknowledge input from Ann Fridlind and Andrew Ackerman. This research was supported by an appointment to the NASA Post-doctoral Program at the NASA Goddard Institute for Space Studies, administered by USRA through a contract with NASA.

References

Abel, S. J., & Boutle, I. A. (2012). An improved representation of the raindrop size distribution for single-moment microphysics schemes. *Quarterly Journal of the Royal Meteorological Society*, 138(669), 2151–2162. <https://doi.org/10.1002/qj.1949>

Albrecht, B. A. (1989). Aerosols, cloud microphysics, and fractional cloudiness. *Science*, 245, 1227–1230. <https://doi.org/10.1126/science.245.4923.1227>

Alexandrov, M. D., Cairns, B., Emde, C., Ackerman, A. S., & van Diedenhoven, B. (2012). Accuracy assessments of cloud droplet size retrievals from polarized reflectance measurements by the research scanning polarimeter. *Remote Sensing of Environment*, 125, 92–111. <https://doi.org/10.1016/j.rse.2012.07.012>

Alexandrov, M. D., Cairns, B., & Mishchenko, M. I. (2012). Rainbow Fourier transform. *Journal of Quantitative Spectroscopy and Radiative Transfer*, 113(18), 2521–2535. <https://doi.org/10.1016/j.jqsrt.2012.03.025>

Alexandrov, M. D., Cairns, B., Sinclair, K., Wasilewski, A. P., Ziemba, L., Crosbie, E., et al. (2018). Retrievals of cloud droplet size from the research scanning polarimeter data: Validation using in situ measurements. *Remote Sensing of Environment*, 210, 76–95. <https://doi.org/10.1016/j.rse.2018.03.005>

Alexandrov, M. D., Miller, D. J., Rajapakse, C., Fridlind, A., van Diedenhoven, B., Cairns, B., et al. (2020). Vertical profiles of droplet size distributions derived from cloud-side observations by the research scanning polarimeter: Tests on simulated data. *Atmospheric Research*, 104924. <https://doi.org/10.1016/j.atmosres.2020.104924>

Austin, P., Wang, Y., Kujala, V., & Pincus, R. (1995). Precipitation in stratocumulus clouds: Observational and modeling results. *Journal of the Atmospheric Sciences*, 52(13), 2329–2352. [https://doi.org/10.1175/1520-0469\(1995\)052<2329:piscoa>2.0.co;2](https://doi.org/10.1175/1520-0469(1995)052<2329:piscoa>2.0.co;2)

Baker, M. B., Corbin, R. G., & Latham, J. (1980). The influence of entrainment on the evolution of cloud droplet spectra: I. A model of inhomogeneous mixing. *Quarterly Journal of the Royal Meteorological Society*, 106(449), 581–598. <https://doi.org/10.1002/qj.49710644914>

Beheng, K. D. (1994). A parameterization of warm cloud microphysical conversion processes. *Atmospheric Research*, 33(1–4), 193–206. [https://doi.org/10.1016/0169-8095\(94\)90020-5](https://doi.org/10.1016/0169-8095(94)90020-5)

Berry, E. X., & Reinhardt, R. L. (1974). An analysis of cloud drop growth by collection: Part I. Double distributions. *Journal of the Atmospheric Sciences*, 31(7), 1814–1824. [https://doi.org/10.1175/1520-0469\(1974\)031<1814:aaocdg>2.0.co;2](https://doi.org/10.1175/1520-0469(1974)031<1814:aaocdg>2.0.co;2)

Brenguier, J.-L., & Chaumat, L. (2001). Droplet spectra broadening in cumulus clouds. Part I: Broadening in adiabatic cores. *Journal of the Atmospheric Sciences*, 58(6), 628–641. [https://doi.org/10.1175/1520-0469\(2001\)058<0628:dsbicc>2.0.co;2](https://doi.org/10.1175/1520-0469(2001)058<0628:dsbicc>2.0.co;2)

Brenguier, J.-L., & Grabowski, W. W. (1993). Cumulus entrainment and cloud droplet spectra: A numerical model within a two-dimensional dynamical framework. *Journal of the Atmospheric Sciences*, 50(1), 120–136. [https://doi.org/10.1175/1520-0469\(1993\)050<0120:ceacds>2.0.co;2](https://doi.org/10.1175/1520-0469(1993)050<0120:ceacds>2.0.co;2)

Cairns, B., Travis, L. D., & Russell, E. E. (1999). The research scanning polarimeter: Calibration and ground-based measurements. *Proceedings of SPIE the International Society for Optical Engineering*, 3754, 186–196.

- Chuang, P. Y., Saw, E. W., Small, J. D., Shaw, R. A., Sipperley, C. M., Payne, G. A., & Bachalo, W. D. (2008). Airborne phase Doppler interferometry for cloud microphysical measurements. *Aerosol Science and Technology*, *42*(8), 685–703. <https://doi.org/10.1080/0278682080232956>
- Comstock, K. K., Wood, R., Yuter, S. E., & Bretherton, C. S. (2004). Reflectivity and rain rate in and below drizzling stratocumulus. *Quarterly Journal of the Royal Meteorological Society*, *130*(603), 2891–2918. <https://doi.org/10.1256/qj.03.187>
- Curry, J. A., & Webster, P. J. (1998). *Thermodynamics of atmospheres and oceans*. Elsevier.
- Dzambo, A. M., L'Ecuyer, T., Sinclair, K., van Diedenhoven, B., Gupta, S., McFarquhar, G., et al. (2020). Joint cloud water path and rainwater path retrievals from ORACLES observations. *Atmospheric Chemistry and Physics Discussions*, 1–44.
- Dzambo, A. M., L'Ecuyer, T., Sy, O. O., & Tanelli, S. (2019). The observed structure and precipitation characteristics of southeast Atlantic stratocumulus from airborne radar during ORACLES 2016–17. *Journal of Applied Meteorology and Climatology*, *58*(10), 2197–2215. <https://doi.org/10.1175/jamc-d-19-0032.1>
- Falkovich, G., Fouxon, A., & Stepanov, M. G. (2002). Acceleration of rain initiation by cloud turbulence. *Nature*, *419*(6903), 151–154. <https://doi.org/10.1038/nature00983>
- Grabowski, W. W., & Wang, L.-P. (2013). Growth of cloud droplets in a turbulent environment. *Annual Review of Fluid Mechanics*, *45*, 293–324. <https://doi.org/10.1146/annurev-fluid-011212-140750>
- Grosvenor, D. P., Sourdeval, O., Zuidema, P., Ackerman, A., Alexandrov, M. D., Bennartz, R., et al. (2018). Remote sensing of droplet number concentration in warm clouds: A review of the current state of knowledge and perspectives. *Reviews of Geophysics*, *56*, 409–453. <https://doi.org/10.1029/2017rg000593>
- Hansen, J. E., & Travis, L. D. (1974). Light scattering in planetary atmospheres. *Space Science Reviews*, *16*(4), 527–610. <https://doi.org/10.1007/bf00168069>
- Hsieh, W. C., Jonsson, H., Wang, L. P., Buzorius, G., Flagan, R. C., Seinfeld, J. H., & Nenes, A. (2009). On the representation of droplet coalescence and autoconversion: Evaluation using ambient cloud droplet size distributions. *Journal of Geophysical Research*, *114*, D07201. <https://doi.org/10.1029/2008jd010502>
- Hudson, J. G., & Yum, S. S. (1997). Droplet spectral broadening in marine stratus. *Journal of the Atmospheric Sciences*, *54*(22), 2642–2654. [https://doi.org/10.1175/1520-0469\(1997\)054<2642:dsbims>2.0.co;2](https://doi.org/10.1175/1520-0469(1997)054<2642:dsbims>2.0.co;2)
- Khain, A. P., & Pinsky, M. (2018). *Physical processes in clouds and cloud modeling*. Cambridge University Press.
- Khairoutdinov, M., & Kogan, Y. (2000). A new cloud physics parameterization in a large-eddy simulation model of marine stratocumulus. *Monthly Weather Review*, *128*(1), 229–243. [https://doi.org/10.1175/1520-0493\(2000\)128<0229:ancppi>2.0.co;2](https://doi.org/10.1175/1520-0493(2000)128<0229:ancppi>2.0.co;2)
- Klein, S. A., & Hartmann, D. L. (1993). The seasonal cycle of low stratiform clouds. *Journal of Climate*, *6*(8), 1587–1606. [https://doi.org/10.1175/1520-0442\(1993\)006<1587:tscols>2.0.co;2](https://doi.org/10.1175/1520-0442(1993)006<1587:tscols>2.0.co;2)
- Kogan, Y., & Ovchinnikov, M. (2020). Formulation of autoconversion and drop spectra shape in shallow cumulus clouds. *Journal of the Atmospheric Sciences*, *77*(2), 711–722. <https://doi.org/10.1175/jas-d-19-0134.1>
- Korolev, A. V. (1994). A study of bimodal droplet size distributions in stratiform clouds. *Atmospheric Research*, *32*(1–4), 143–170. [https://doi.org/10.1016/0169-8095\(94\)90057-4](https://doi.org/10.1016/0169-8095(94)90057-4)
- Korolev, A. V. (1995). The influence of supersaturation fluctuations on droplet size spectra formation. *Journal of the Atmospheric Sciences*, *52*(20), 3620–3634. [https://doi.org/10.1175/1520-0469\(1995\)052<3620:tiosfo>2.0.co;2](https://doi.org/10.1175/1520-0469(1995)052<3620:tiosfo>2.0.co;2)
- Lasher-trapp, S. G., Cooper, W. A., & Blyth, A. M. (2005). Broadening of droplet size distributions from entrainment and mixing in a cumulus cloud. *Quarterly Journal of the Royal Meteorological Society: A Journal of the Atmospheric Sciences, Applied Meteorology and Physical Oceanography*, *131*(605), 195–220
- Lebsock, M. D., & L'Ecuyer, T. S. (2011). The retrieval of warm rain from CloudSat. *Journal of Geophysical Research*, *116*, D20209. <https://doi.org/10.1029/2011jd016076>
- Lebsock, M. D., L'Ecuyer, T. S., & Stephens, G. L. (2011). Detecting the ratio of rain and cloud water in low-latitude shallow marine clouds. *Journal of Applied Meteorology and Climatology*, *50*(2), 419–432. <https://doi.org/10.1175/2010jamc2494.1>
- L'Ecuyer, T. S., & Stephens, G. L. (2002). An estimation-based precipitation retrieval algorithm for attenuating radars. *Journal of Applied Meteorology*, *41*(3), 272–285. [https://doi.org/10.1175/1520-0450\(2002\)041<0272:aebpra>2.0.co;2](https://doi.org/10.1175/1520-0450(2002)041<0272:aebpra>2.0.co;2)
- Liou, K.-N., & Ou, S.-C. (1989). The role of cloud microphysical processes in climate: An assessment from a one-dimensional perspective. *Journal of Geophysical Research*, *94*(D6), 8599–8607. <https://doi.org/10.1029/jd094id06p08599>
- Long, A. B., & Manton, M. J. (1974). On the evaluation of the collection kernel for the coalescence of water droplets. *Journal of the Atmospheric Sciences*, *31*(4), 1053–1057. [https://doi.org/10.1175/1520-0469\(1974\)031<1053:ototec>2.0.co;2](https://doi.org/10.1175/1520-0469(1974)031<1053:ototec>2.0.co;2)
- Martins, J. V., Fernandez-Borda, R., McBride, B., Remer, L., & Barbosa, H. M. J. (2018). The HARP hyperangular imaging polarimeter and the need for small satellite payloads with high science payoff for Earth science remote sensing. *IEEE International Geoscience and Remote Sensing Symposium*, 6304–6307.
- McBride, B. A., Martins, J. V., Barbosa, H. M. J., Birmingham, W., & Remer, L. A. (2019). Spatial distribution of cloud droplet size properties from airborne hyper-angular rainbow polarimeter (AirHARP) measurements. *Atmospheric Measurement Techniques*, *13*, 1777–1796.
- Miller, D. J., Zhang, Z., Platnick, S., Ackerman, A. S., Werner, F., Cornet, C., & Knobelspiesse, K. (2018). Comparisons of bispectral and polarimetric retrievals of marine boundary layer cloud microphysics: Case studies using a LES-satellite retrieval simulator. *Atmospheric Measurement Techniques*, *11*(6), 3689–3715. <https://doi.org/10.5194/amt-11-3689-2018>
- Morrison, H., van Lier-Walqui, M., Fridlind, A. M., Grabowski, W. W., Harrington, J. Y., Hoose, C., et al. (2020). Confronting the challenge of modeling cloud and precipitation microphysics. *Journal of Advances in Modeling Earth Systems*, *12*, e2019MS001689. <https://doi.org/10.1029/2019MS001689>
- Nakajima, T., & King, M. D. (1990). Determination of the optical thickness and effective particle radius of clouds from reflected solar radiation measurements. Part I: Theory. *Journal of the Atmospheric Sciences*, *47*(15), 1878–1893. [https://doi.org/10.1175/1520-0469\(1990\)047<1878:dotota>2.0.co;2](https://doi.org/10.1175/1520-0469(1990)047<1878:dotota>2.0.co;2)
- Nakajima, T. Y., Suzuki, K., & Stephens, G. L. (2010a). Droplet growth in warm water clouds observed by the A-Train. Part I: Sensitivity analysis of the MODIS-derived cloud droplet sizes. *Journal of the Atmospheric Sciences*, *67*(6), 1884–1896. <https://doi.org/10.1175/2009jas3280.1>
- Nakajima, T. Y., Suzuki, K., & Stephens, G. L. (2010b). Droplet growth in warm water clouds observed by the A-Train. Part II: A multisensor view. *Journal of the Atmospheric Sciences*, *67*(6), 1897–1907. <https://doi.org/10.1175/2010jas3276.1>
- Painemal, D., & Zuidema, P. (2011). Assessment of MODIS cloud effective radius and optical thickness retrievals over the Southeast Pacific with VOCALS-REx in situ measurements. *Journal of Geophysical Research*, *116*, D24206. <https://doi.org/10.1029/2011jd016155>
- Pawlowska, H., & Brenguier, J. L. (2003). An observational study of drizzle formation in stratocumulus clouds for general circulation model (GCM) parameterizations. *Journal of Geophysical Research*, *108*, 8630. <https://doi.org/10.1029/2002jd002679>

- Pinsky, M., Khain, A., & Shapiro, M. (2001). Collision efficiency of drops in a wide range of Reynolds numbers: Effects of pressure on spectrum evolution. *Journal of the Atmospheric Sciences*, 58(7), 742–764. [https://doi.org/10.1175/1520-0469\(2001\)058<0742:ceodia>2.0.co;2](https://doi.org/10.1175/1520-0469(2001)058<0742:ceodia>2.0.co;2)
- Pinsky, M. B., & Khain, A. P. (2002). Effects of in-cloud nucleation and turbulence on droplet spectrum formation in cumulus clouds. *Quarterly Journal of the Royal Meteorological Society*, 128(580), 501–533. <https://doi.org/10.1256/003590002321042072>
- Pinsky, M. B., Khain, A. P., & Shapiro, M. (2007). Collisions of cloud droplets in a turbulent flow. Part IV: Droplet hydrodynamic interaction. *Journal of the Atmospheric Sciences*, 64(7), 2462–2482. <https://doi.org/10.1175/jas3952.1>
- Prabha, T. V., Khain, A., Maheshkumar, R. S., Pandithurai, G., Kulkarni, J. R., Konwar, M., & Goswami, B. N. (2011). Microphysics of premonsoon and monsoon clouds as seen from in situ measurements during the Cloud Aerosol Interaction and Precipitation Enhancement Experiment (CAIPEEX). *Journal of the Atmospheric Sciences*, 68(9), 1882–1901. <https://doi.org/10.1175/2011jas3707.1>
- Pruppacher, H. R., & Klett, J. D. (1997). *Microphysics of Clouds and precipitation*. Kluwer Academic Publishers. Atmospheric and Oceanographic Sciences Library.
- Pruppacher, H. R., & Klett, J. D. (2010). Microstructure of atmospheric clouds and precipitation. In *Microphysics of clouds and precipitation*. Dordrecht: Springer.
- Redemann, J., Wood, R., Zuidema, P., Doherty, S. J., Luna, B., LeBlanc, S. E., et al. (2020). An overview of the ORACLES (ObseRvations of Aerosols above CLouds and their intERactions) project: aerosol-cloud-radiation interactions in the Southeast Atlantic basin. *Atmospheric Chemistry and Physics Discussions*, 1–82.
- Segal, Y., Pinsky, M., Khain, A., & Erlick, C. (2003). Thermodynamic factors influencing bimodal spectrum formation in cumulus clouds. *Atmospheric Research*, 66(1–2), 43–64. [https://doi.org/10.1016/s0169-8095\(02\)00172-2](https://doi.org/10.1016/s0169-8095(02)00172-2)
- Sinclair, K., van Diedenhoven, B., Cairns, B., Alexandrov, M., Moore, R., Ziemba, L. D., & Crosbie, E. (2020). Observations of aerosol-cloud interactions during the North Atlantic aerosol and marine ecosystem study. *Geophysical Research Letters*, 47, e2019GL085851. <https://doi.org/10.1029/2019gl085851>
- Sinclair, K., Van Diedenhoven, B., Cairns, B., Yorks, J., Wasilewski, A., & McGill, M. (2017). Remote sensing of multiple cloud layer heights using multi-angular measurements. *Atmospheric Measurement Techniques*, 10(6), 2361. <https://doi.org/10.5194/amt-10-2361-2017>
- Takahashi, H., Lebsock, M., Suzuki, K., Stephens, G., & Wang, M. (2017). An investigation of microphysics and subgrid-scale variability in warm-rain clouds using the A-Train observations and a multiscale modeling framework. *Journal of Geophysical Research: Atmospheres*, 122, 7493–7504. <https://doi.org/10.1002/2016jd026404>
- Wallace, J. M., & Hobbs, P. V. (2006). *Atmospheric science: An introductory survey*. Elsevier.
- Warner, J. (1969a). The microstructure of cumulus cloud. Part I. General features of the droplet spectrum. *Journal of the Atmospheric Sciences*, 26(5), 1049–1059. [https://doi.org/10.1175/1520-0469\(1969\)026<1049:tmoccp>2.0.co;2](https://doi.org/10.1175/1520-0469(1969)026<1049:tmoccp>2.0.co;2)
- Warner, J. (1969b). The microstructure of cumulus cloud. Part II. The effect on droplet size distribution of the cloud nucleus spectrum and up-draft velocity. *Journal of the Atmospheric Sciences*, 26(6), 1272–1282. [https://doi.org/10.1175/1520-0469\(1969\)026<1272:tmoccp>2.0.co;2](https://doi.org/10.1175/1520-0469(1969)026<1272:tmoccp>2.0.co;2)
- Werdell, P. J., Behrenfeld, M. J., Bontempi, P. S., Boss, E., Cairns, B., Davis, G. T., et al. (2019). The Plankton, aerosol, cloud, ocean ecosystem mission: Status, Science, Advances. *Bulletin of the American Meteorological Society*, 100(9), 1775–1794. <https://doi.org/10.1175/bams-d-18-0056.1>
- Wood, R. (2005a). Drizzle in stratiform boundary layer clouds. Part I: Vertical and horizontal structure. *Journal of the Atmospheric Sciences*, 62(9), 3011–3033. <https://doi.org/10.1175/jas3529.1>
- Wood, R. (2005b). Drizzle in stratiform boundary layer clouds. Part II: Microphysical aspects. *Journal of the Atmospheric Sciences*, 62(9), 3034–3050. <https://doi.org/10.1175/jas3530.1>